HHS Public Access

Author manuscript

Circ Arrhythm Electrophysiol. Author manuscript; available in PMC 2020 February 22.

Published in final edited form as:

Circ Arrhythm Electrophysiol. 2016 April ; 9(4): e004133. doi:10.1161/CIRCEP.116.004133.

Myofiber Architecture of the Human Atria as Revealed by Sub-Millimeter Diffusion Tensor Imaging

Farhad Pashakhanloo, BSc[1], **Daniel A. Herzka, PhD**[1], **Hiroshi Ashikaga, MD, PhD**[2], **Susumu Mori, PhD**[3], **Neville Gai, PhD**[4], **David A. Bluemke, MD**[4], **Natalia A. Trayanova, PhD**[1], **Elliot R. McVeigh, PhD**[1,3,5]

[1]Department of Biomedical Engineering, Johns Hopkins University, Baltimore

[2]Department of Medicine, Johns Hopkins University, Baltimore

[3]Department of Radiology, Johns Hopkins University, Baltimore

[4]Radiology and Imaging Sciences, National Institute of Health Clinical Center, Bethesda, MD

[5]Departments of Bioengineering, Medicine, Radiology, University of California, San Diego, La Jolla, CA

Abstract

Background—Accurate knowledge of the human atrial fibrous structure is paramount in understanding the mechanisms of atrial electrical function in health and disease. Thus far such knowledge has been acquired from destructive sectioning, and there is a paucity of data regarding atrial fiber architecture variability in the human population.

Methods and Results—In this study, we have developed a customized 3D diffusion tensor magnetic resonance imaging (DTMRI) sequence on a clinical scanner that makes it possible to image an entire intact human heart specimen *ex vivo* at sub-millimeter resolution. The data from eight human atrial specimens obtained with this technique present complete maps of the fibrous organization of the human atria. The findings demonstrate that the main features of atrial anatomy are mostly preserved across subjects, although the exact location and orientation of atrial bundles vary. Using the full tractography data, we were able to cluster, visualize, and characterize the distinct major bundles in the human atria. Further, quantitative characterization of the fiber angles across the atrial wall revealed that the transmural fiber angle distribution is heterogeneous throughout different regions of the atria.

Conclusions—The application of sub-millimeter DTMRI provides an unprecedented level of information regarding both human atrial structure as well as its inter-subject variability. The high resolution and fidelity of this data could enhance our understanding of structural contributions to atrial rhythm and pump disorders, and lead to improvements in their targeted treatment.

Correspondence: Elliot R. McVeigh, PhD, Departments of Bioengineering, Medicine, Radiology, University of California, San Diego, 9500 Gilman Drive – MC0412, La Jolla, CA 92093-0412, Tel: 410-598-1526, Fax: 858-246-0167, emcveigh@ucsd.edu.

Disclosures: NT is a cofounder of CardioSolv, LLC and EM is a cofounder and shareholder of MR Interventions Inc. CardioSolv and MR Interventions were not involved in this research.

Keywords

atrium; arrhythmia (mechanisms); myofiber; structure; diffusion tensor imaging; Arrhythmias; Atrial Fibrillation; Electrophysiology; Mechanisms; Magnetic Resonance Imaging (MRI)

Introduction

The exact relation between atrial structural pathways and electrical function/dysfunction in normal and diseased human atria has not been fully charactrized[1]. Atrial muscular architecture has a direct effect on atrial electrical activity by creating a preferential direction for excitation wave propagation[2] and has been shown to promote rhythm disturbances under a variety of conditions [3–8]. Therefore, accurate knowledge of the human atrial fibrous structure is important in understanding human atrial arrhythmia mechanisms; such knowledge could contribute significantly towards the improvement of strategies for treating atrial rhythm disorders[9].

Existing information regarding atrial fiber orientation has been acquired from photography and tracings of visually observed tracts after sectioning the atria[10–13]. In addition to being destructive to the tissue and thus possibly introducing measurement biases, such methodologies involve the cumbersome task of reconstructing the 3D atrial structure from piece-wise data[14]; this task is particularly difficult for the large human atria. Furthermore, such acquisition methods render the systematic inter-subject comparison nearly impossible. Consequently, in contrast to the ventricles, there is a paucity of data regarding atrial fiber architecture variability in the human population. The need for such data is underscored by the fact that atrial anatomy varies greatly in the human population, as documented by *in-vivo* imaging[15,16]

Diffusion Tensor Magnetic Resonance Imaging (DTMRI) is a non-invasive technique that uses water diffusion as a probe to image fiber orientation in tissue[17,18]. DTMRI has been widely utilized to study fiber architecture in the brain and other organs[19,20]. Importantly, it has been successfully applied to acquire ventricular fiber orientations in normal and diseased hearts, both in animal species and in the human[21–25]. Ventricular fiber maps derived from DTMRI have been shown to correspond well to histological measurements of fiber angles[26–29]. Acquiring DTMRI atrial fiber architecture, however, has proven extremely challenging. Difficulties arise from the fact that the atrial wall is significantly thinner than the ventricular wall, and from the high complexity of atrial fiber architecture, consisting of overlapping and interconnected bundles running throughout the chambers. Successful acquisition of atrial fiber architecture thus necessitates very high DTMRI image resolution and quality.

In this study, we present the first DTMRI acquisition of fiber architecture in the human atria. We have developed a customized 3D DTMRI sequence on a clinical scanner that makes it possible to image an entire intact human heart specimen *ex vivo*. We have optimized the MRI sequence so that the scan can be performed over a long period of time without deterioration in image stability. The method yields both high image signal-to-noise ratio (SNR) and resolution, which are essential for capturing details in atrial structure. Here, we

applied this new technique to reconstruct the 3D fiber orientation in eight human atria at a sub-millimeter resolution, providing an unprecedented level of information regarding both human atrial structure as well as its inter-subject variability. The information obtained in this study could lead to an enhanced understanding of atrial rhythm and pump disorders and thus improvements in their targeted treatment. The new DTMRI methodology is also expected to have broad utilization in acquiring the structure of other large specimens at sub-millimeter resolution.

Methods

Specimen acquisition and preparation

Human hearts (including the intact atria) were procured through the National Disease Research Interchange (NDRI, Philadelphia, PA). The hearts were from donors between the ages of 50 and 100 years (n=8, see Table 1 for donor characteristics). The tissue post mortem recovery interval was 12 hours. Diffusion imaging over a long time interval demands specimen preparation that ensures minimal artifact as well as sample stability during acquisition. In this study, the hearts were fixed in 10% buffered formaldehyde post recovery and were submerged in a buffer prior to imaging. In order to assure complete fixation of the whole heart, the specimens were scanned at least 40 days after the onset of the fixation in the formaldehyde. The atria were carefully filled and shaped, without damaging the tissue, to be close to the LV end-systolic state (maximum atrial filling) using compressed cotton absorbent. During acquisition, to obtain zero background signal from the heart chambers while avoiding specimen dehydration and susceptibility artifacts generated from the a tissue-air interface, the hearts were submerged in a perfluorocarbon solution (3M, Maplewood, Minnesota). Test scans were performed to detect and eliminate any air bubble artifact inside the atria. The images from the beginning and the end of the experiment were compared to confirm the negligible change in the level of the tissue signal and in the specimen position over the long duration of scan (see Supplementary Methods).

Imaging

The primary challenge for this project was to create a pulse sequence with sufficient resolution and diffusion sensitivity to image detail within the atrial wall, while retaining the imaging stability over the MRI scan time which averaged approximately 50 hours per specimen. The large specimen size of the *ex vivo* heart required a clinical scanner (3T Achieva TX, Philips Healthcare, Best, Netherlands). The RF coil used in this study was Philips 8-Channel head coil. The balance between high gradient amplitudes, and optimized imaging bandwidth for artifact reduction was found through a series of iterative trials. The final sequence used was a 3D Fast Spin Echo: TE = 60ms, TR = 625 ms, BW = 289.8Hz/pixel, number of echoes = 2, partial echo factor = 0.6, diffusion gradients duration = 22.9 ms, time gap between diffusion pulses = 12.5 ms, max gradient strength = 60 mT/m, number of diffusion encoding directions = 15, maximum b-value = 800 s/mm^2, FOV: 110×90×120 mm^3 (covering the whole heart), acquired voxel dimension: 0.5×0.5×1.0 mm^3. The images were reconstructed with 0.4mm^3 isotropic voxels by using zero padding. The measured SNR for the non-diffusion weighted images (b0) was ~120 (+/− 20). The 1.0 mm “slice” direction of the voxels was aligned with the longitudinal axis of the heart.

To achieve high accuracy in the segmentation of the thin atrial wall, specimens were additionally imaged using a 3D T1-weighted gradient echo MRI at an isotropic resolution of $0.25mm^3$ (TE=2.3ms, TR=12ms, scan duration: 1hr). These higher resolution images were used to guide the segmentation process.

Post processing

Raw MRI data were exported from the scanner and a customized image reconstruction was performed offline using MATLAB (The MathWorks Inc., Natick, MA) scripts. The reconstruction took advantage of the two spin-echoes to increase the SNR of the final diffusion images. From the 15 diffusion encoded images and the b0 image, diffusion tensors were calculated using DTI Studio[30]. The atrial myocardium was segmented semi-automatically using manual thresholding and masking of the b0 image in combination with the T1 weighted image. Fractional Anisotropy (FA) is a scalar measure of diffusion anisotropy pattern in the tissue and ranges between 0 (fully isotropic diffusion) and 1 (fully anisotropic diffusion). Low and high cut-off thresholds were applied to the FA map (inclusion range: 0.01 – 0.45) to exclude the low-quality voxels (e.g. voxels with partial volume artifact, fat, tissue decomposition) that generate extreme FA values. These segmentation masks defined the boundaries for the measurement of fiber angles and other structural properties in the atrium.

Fiber angle measurement

A contribution of this work is the discovery of a reproducible coordinate system to express the relative fiber angles of the myocardial tracts on the roof of the LA. To do so, the origins of the 4 pulmonary veins were used as the reference points within the highly complex geometry of the atria. A “horizontal” vector was defined, connecting the median points of the left (inferior and superior) and right (inferior and superior) PVs, as shown in Figure 2. Once this coordinate system was established for each atrium, the principal eigenvectors were projected onto the local plane that is tangential to the atrial surface at the closest point. The fiber angles on the roof of the left atria were defined as the angle between the projected eigenvector and the projection of the horizontal vector onto the same tangential plane. In this coordinate system the fibers with an angle of 0° run left to right on the roof of the LA, and fibers extending in the anterior-posterior direction have fiber angle of 90°, as shown in the cartoon at the bottom right of Figure 2. For each heart, a ~2×2 cm patch was defined at the center of the atrial roof to measure the mean fiber angle on the roof (see schematic at bottom of Figure 2).

Maps of transmural fiber angle dispersions were created by calculating the angular deviations of local fiber angles inside a disk with diameter 4mm that goes through the entire atrial wall, regardless of wall thickness.

Tractography

For the purpose of visualization, fiber tracking was performed on the principal eigenvector using the Fiber Assignment by Continuous Tracking (FACT) algorithm[30] (stopping criteria: FA = 0.065, angle deviation = 45 degrees) in DTI Studio. The resulting tracts are a macroscopic manifestation of fiber architecture and are locally aligned with the myofibers.

The fibers were rendered using Trackvis software[31] (see Supplementary Methods for detailed visualization pipeline). The individual points on the fibers tracts were then color-coded based on their absolute distance from the endocardial shell (red: epicardial, yellow: endocardial).

In order to group the fiber tracts into the new basis set of "bundles" that are common to all atria, semi-automatic clustering was performed based on the similarity in the orientation of the neighboring tracts. An initial k-means algorithm was applied to regroup the tracts into a number of clusters (n>50), each containing adjacent tracts with similar fiber orientations. These clusters were then manually selected in TrackVis, by placing seed points on the atria and finding the tracts that intersect them. Total of 15 "basis" bundles were selected using this technique, each with a distinct orientation and spatial extent.

Results

As described in the Methods, all images were acquired with voxel resolution of $0.5\times0.5\times1.0mm^3$ and reconstructed to $0.4\times0.4\times0.4mm^3$. The average thickness of the atrial wall across the eight human atria was 2.73mm (5–95% quartiles: 0.98–4.38mm), which corresponds to 4.34 voxels (5–95% quartiles: 1.56–6.96 voxels). The mean Fractional Anisotropy (FA, see Methods) and Mean Diffusivity (MD) in the sampled atria were 0.18 (25–75% quartiles: [0.12–0.22]) and 8.5×10^{-4} mm^2/s (25–75% quartiles: $[6.8–10.1]\times10^{-4}$ mm^2/s) respectively. The corresponding values for FA and MD measured in LVs of the same hearts were 0.20 (25–75% quartiles: [0.15–0.23]) and 7.3×10^{-4} mm^2/s (25–75% quartiles: $[6.3–8.1]\times10^{-4}$ mm^2/s). Figure 1A,B presents data from two samples, illustrating the complexity of human atrial geometry. Figure 1A shows a short axis slice (b0 image, non-diffusion weighted) with the superimposed segmentation of atrial tissues (left and right atria, and the inter-atrial bundle). In Figure 1B, atrial geometry is rendered by the grey volume of the lumen. All main features of atrial structure, including the pulmonary veins (PVs) and the trabeculated surfaces of left and right atrial appendages have been captured at this resolution.

The 3D spatial organization of myofiber architecture was visualized using fiber tractography (see Methods). Figure 1C–F presents renderings of the fiber architecture in the same human atrial specimen from different anatomical viewpoints. The color at each point on the tract represents the shortest local distance to the endocardial shell and is used to illustrate the depth of the fiber tracts across the atrial wall (yellow on the endocardium, red on the epicardium). Fiber tracts were found to have varying lengths and local densities (see Methods), and to be at different distances from the lumen. As the figure demonstrates, fibers traveling in different directions cross over or transition into each other throughout the atrial wall. The presented images illustrate the complexity of atrial fiber architecture in the three-dimensional (3D) organ.

Fiber tractography results were obtained for all 8 human atrial specimens, as described in Methods. Figure 2 presents tractography for the roof of each left atrium (LA, posterior aspect). To assess inter-subject variability in fiber orientation in this region of the atria, fiber angles were measured using a coordinate system constructed from the 4 origins of the

pulmonary veins, as described in Methods (see schematic at bottom of Figure 2). Results (Table 1) reveal a dominant longitudinal orientation of fibers at the LA roof in 7 of the 8 specimens; the average fiber angle for the 7 specimens (excluding Heart 3) was 99 degrees, with a *very* small standard deviation of 3 degrees. Heart 3 is uniquely different from the other samples. It contains a mixture of longitudinal and oblique fibers at the LA roof (mean angle of 168 degrees).

We next studied the fiber architecture across the depth of the atrial wall. Figure 3 demonstrates the fibers at different transmural layers of human atria as viewed from posterior and anterior sides, using sub-endocardial and sub-epicardial cuts. Further characterization of regional changes in fiber orientation across the atrial wall in 8 specimens is presented in Figure 4. Fiber tractography in posterior and anterior views of specimen 4 and 1 are shown in Figure 4A,C, respectively. In Figure 4A, top, two regions of interest (ROI), each of radius 4mm, are delineated; they are ~16mm apart. Histograms display the *transmural* distribution of fiber angles in each ROI (Figure 4A, middle row). The bimodal distribution of angles in ROI A (located closer to the left inferior PV) demonstrates the presence of two layers of distinct local fiber orientations across the wall -- the fiber layers run in perpendicular directions. This change in fiber angles in direction from epi- to endocardium takes place abruptly at the midwall (Figure 4A, bottom). ROI B shows a unimodal distribution of fiber angles that is mainly oriented along the medial axis of the posterior wall. Similar findings are presented in Figure 4C,D.

The pattern of fiber architecture with two distinct layers of different (nearly perpendicular) orientations across the wall was observed at several locations in the atria. To better assess fiber structure in the depth of the atrial wall, we quantified the transmural fiber dispersion throughout the atrial wall in each specimen by the angular deviation of the local fiber angles (see Methods). The angular deviation was color-coded and mapped onto the corresponding atrial lumen surface (Figure 4B,D). There was a dominant unimodal transmural fiber pattern at the LA roof of 4 of the atria (specimens 1,5,6 and 7). The remaining specimens were characterized with fiber patterns of higher transmural dispersion in orientation, particularly near the PVs. In all samples, the inferior and anterior sides of the left atria exhibited a high dispersion in transmural fiber angles, while the lateral wall of the left atria below the left PVs had consistently a unimodal transmural fiber distribution.

As demonstrated above, tractography results revealed the presence of fiber tracts with varying spatial extent and orientation throughout the atria. Our analysis demonstrated that groups of neighboring tracts running in the same direction tend to form major bundles that in some cases constitute distinct anatomical features of atrial muscular architecture. We used a semi-automatic algorithm to cluster distinct bundles from the full tractography data (see Methods). The results for specimen 7 are presented in Figure 5, demonstrating 15 distinct major bundles (labeled a-l). Importantly, presence of these major bundles was consistent across most of the specimens despite variation in cardiovascular clinical status of the subjects. For instance, two of the patients in this study had recorded history of atrial fibrillation (Hearts 6 and 7); our measurements showed larger left atrial blood volumes for these two patients in comparison to the rest of the population. Despite this, we did not find any conspicuous differences in the fiber architecture of these two specimens when compared

to the rest of the hearts; the general patterns of major fiber bundles (Figure 5) were observed in these two samples as well. The description of the major bundles follows below, presented in the context of their place within the overall 3D atrial architecture, and in relation to known atrial structures[11,12].

The major fiber orientation on the posterior wall of the left atria was found to be posterior-to-anterior (Figure 1C and Figure 5B - bundle **c,** recognized in the literature as Septopulmonary bundle[32]). On the left and the right, this bundle transitions toward the bundles that encircle the base of each PV (bundles a_1 through a_4). A group of fibers on the inferior-posterior and lateral side of left atrial wall (bundles **b** and **d** in Figure 5A,C) run circumferentially around the “waist” of the LA, crossing, on the posterior wall, over the Septopulmonary bundle (see also Figure 1E).

A pattern of overlapping fiber bundles was observed consistently on the anterior side of all the human atrial specimens (Figure 1D, Figure 5D,E)[11]. One dominant fiber bundle on this side was the inter-atrial band, which originates below the superior vena cava (SVC) in the right atrium (RA) and bridges the LA (known as Bachman Bundle[33], Figure 5E bundle **l**). The extension of the Bachman Bundle on the left side of the LA splits into two bands that run around the LAA (Figure 4D bundle **h** and Figure 5E bundle **b**). The inferior part of the anterior wall in proximity to the mitral valve consists of oblique and circumferential bundles (Figure 5D,E). These bundles represent extensions of fiber tracts from the LA roof and lateral wall (Figure 5D bundles **g** and **i**, respectively). The superior side of the anterior wall contains another oblique bundle that originates from the base of the left superior pulmonary vein (LSPV) and runs toward the septum below the right superior pulmonary vein (RSPV, Figure 5E, bundle **j**). The extension of this bundle continues through the inferior septum (bundle **k** in Figure 5E,F).

The septal wall incorporates circumferentially-running fibers that extend from the posterior wall (Figure 5F, bundle **e**), as well as obliquely-running fibers originating between the right PVs (Figure 5F, bundle **f**). Depicted in Figure 5F, the Oval Fossa (OF) is a known distinct structural feature of the septal wall[11]. Fibers run circumferentially inferior to OF and extend to the posterior and anterior walls via the extension of bundles **c** and **k,** respectively (Figure 5F). There is also a distinct group of fibers from the RA that run circumferentially around the OF center (Figure 5F).

The right atrial wall contains the specialized structures of the crista terminalis (CS) and pectinate muscles (PM)[11]. These structures manifest themselves in the tractography results as dense parallel bundles (Figure 1F and Figure 6B). As seen in Figure 1F, PMs run longitudinally throughout the wall and transition into CS bundles. The CS bundles are oriented in the inferior-to-superior vena cava direction and extend below SVC on the anterior side. The orientation of these fiber tracts generally follows the trabeculated structure of the endocardial wall (Figure 6).

Discussion

In this study we reconstructed the 3D myofiber organization in human atria non-destructively and at sub-millimeter resolution. To do so, we developed a high-resolution optimized 3D diffusion tensor MR technique on a clinical scanner (to accommodate the large specimens) and imaged the fiber architecture in eight human hearts *ex vivo*. The novel sequence and sample preparation allowed us to acquire the data over long scanning times with high image stability and high SNR. Using the technique, we were able to trace and characterize major bundles individually, and importantly, to present the relation between the various structures in the context of the overall 3D atrial fiber architecture. The sub-millimeter resolution of the data provided information regarding local myofiber orientation across the atrial wall as well as the spatial heterogeneity of transmural fiber angle dispersion throughout the whole atria. The data presented in Figures 1 and 2 portray the first complete maps of atrial fibers in the entire atria. Furthermore, acquiring data on eight human atrial specimens allowed us to study the variability and similarity of the observed patterns across subjects.

The inter-subject analysis of the fiber architecture demonstrated that the main features of atrial anatomy are mostly preserved across subjects, although the exact location and the orientation of the bundles vary from heart to heart. The dominant feature on the roof of the atria is the longitudinal fibers that transition to a circular pattern encircling the four pulmonary veins (Figure 1C and Figure 2). These “vertical” bundles were clearly observed in 7 of the 8 hearts of the study. However, in one of the hearts a mixed pattern of oblique and horizontal fibers was present on the roof (Figure 2 – Heart 3). Nathan et al[10] studied variability of superficial fibers at the junctions of the PVs in 16 postmortem hearts using dissection and visual tracing in the 1960s. They also observed the presence of mixed and oblique pattern of fibers in their population and reported that the most frequent fiber pattern on the roof was longitudinal, which is consistent with our findings. The systematic measurement of myocardial architecture properties such as fiber angles requires the definition of a coordinate system (or systems) in the atria that is reproducible across subjects with various atrial morphologies. This has been suggested previously for the ventricles[34] but is particularly difficult for the atria due to their complex shape. Our findings show that in 7 of the 8 specimens there exists a coordinate system in each LA that is based on the origins of the PVs, and in which major fiber bundles runs in the same orientation (within 3 degrees) on the roof and posterior wall. These findings suggest that this PV-based coordinate system (or a variation of it) could be an intrinsic choice for systematic measurements in the atrium.

The atrial wall has been previously suggested to have a bilayer structure, with fibers in the epicardial and endocardial layers running in nearly perpendicular directions. Evidence for this comes from either measurements undertaken at the tissue level[6] or qualitative descriptions at the organ level[12]. The data obtained from DTMRI here enabled us to “see through” the atrial wall (Figure 3) and perform quantitative measurement and characterization of the local transmural fiber distribution throughout the atria. Bilaminar muscular architecture was indeed documented by DTMRI in the posterior-inferior and anterior regions; however, in the lateral wall and the roof of the LA the fiber angles were

essentially constant from endocardium to epicardium (Figure 4). This analysis demonstrated that the transmural fiber angle distribution in the atria is regionally heterogeneous.

The new knowledge obtained from this study can help interpret with greater accuracy experimental and clinical findings about the functioning of the atria and help better elucidate the link between electrophysiological and electromechanical activity, and the structural features in the normal and diseased atria. Of particular importance is the role of atrial structural organization and heterogeneous fiber orientation in rhythm disorders, as explored by a number of experimental and clinical studies [2,5,7,8,35,36]. For instance, characterization of left atrial activation in human subjects has revealed that the change in fiber orientation and wall thickness at the boundary of the Septopulmonary bundles in the posterior could lead to conduction block during sinus rhythm propagation[36]. The same structural features have been shown to be substrate for atrial fibrillation initiation following rapid burst pacing at the PVs in normal sheep hearts[7]. In the right atrium, the branching sites of the CT and PM were found to cause frequency-dependent breakdown of wave propagation into fibrillatory conduction[8]. The results of our study could be employed to gain further insights into the structural contributions of atrial activity in health and disease. For instance, we can speculate that the spatial variation of transmural dispersion (Figure 4) could promote local conduction disturbances as the wave travels from a region with a more uniform transmural fiber orientation to a region with a bimodal distribution, particularly under conditions of decreased excitability. Such spatial heterogeneity in fiber orientation could also modulate the dynamics and localization of atrial rotors underlying human atrial fibrillation[37,38].

Accurate human atrial fiber orientation data is essential for the construction of computational models of the whole human atria[14,39,40], and the need for it has been acknowledged in numerous studies[41–45]. The DTMRI results presented here provide unprecedented detail about fiber architecture that can easily by incorporated in atrial models by co-registration and morphing methodologies[25,46]. The presented set of the major bundles (Figure 5) in combination with information about wall-thickness and transmural distribution of fiber orientation could form the basis for an accurate mathematical reconstruction of atrial fiber architecture (i.e. a rule-based approach, comprising of fiber orientation “rules” based on the present data) thus enabling atrial model construction from purely geometrical data (e.g. CT or MRI scans) of individual patient atria. The discovery of a common coordinate system and set of reproducible fiber bundles among specimens, as demonstrated here, could facilitate this approach. The integration of detailed structural data into computational models of whole human atria could further help identify the role of individual atrial structures in human arrhythmogenesis under various conditions. Furthermore, patient-specific atrial models are being constructed with the goal of identifying the optimal ablation targets for atrial flutter and fibrillation in an individualized way[43]. Incorporation of accurate fiber orientation will ensure improved accuracy in these clinical translation-bound modeling efforts.

The present study could have important implications for the design of methodologies for the acquisition of atrial fiber architectures in patients. Despite the increasing number of attempts at *in vivo* DTMRI for assessing myofiber structure in the left ventricle, diffusion imaging of a beating heart remains extremely challenging, with many co-founding factors, such as bulk

motion and myocardial strain, that can affect the measured signal[47–49]. The thin wall and the complex pattern of fibers in the atria present additional challenges to this task as compared to the ventricles. However, we can speculate that given a strong baseline knowledge of the fiber patterns in the human atrium, such as obtained in the present study, one could design a diffusion weighted sequence to detect those patterns in selected regions of the atria *in vivo*. This would require the rational design of imaging volumes and voxel orientations to include resolvable sections of the atria in each patient. The *ex vivo* data obtained in this study would inform the definition of those resolvable sections, and therefore, would facilitate a targeted imaging of the atrial fiber structure in patients.

Limitations

Despite the sub-millimeter resolution of our DTMRI imaging, with ~4.5 voxels across the atrial wall in most sections, those sections with thickness less than 0.5 mm could not be reliably imaged; these very thin areas were usually located in the extension of the veins and occasionally in portions of the right atrial wall. Furthermore, while we were able to characterize consistent fiber orientation patterns across the atrial specimens, the advanced age of the donors (55–94 years) and their history of cardiac disease may render our findings not entirely applicable to the atria structure of the general population. Finally, the number of subjects studied here is small and thus the findings may not reflect the true population diversity. The limited number of donor hearts also limited our ability to study the link between structural properties and disease state; however, we believe this study sets the groundwork for such investigations in the future.

Supplementary Material

Refer to Web version on PubMed Central for supplementary material.

Acknowledgments

Authors would like to thank Dr. Henry Bryant for assisting on the coordination of the long duration MRI experiments.

Sources of Funding: The authors acknowledge support by the National Institutes of Health Director’s Pioneer Award to NT (DP1HL123271) and the NIH intramural research program.

References

1. Schotten U, Verheule S, Kirchhof P, Goette A. Pathophysiological mechanisms of atrial fibrillation: a translational appraisal. Physiol Rev. 2011;91:265–325. [PubMed: 21248168]
2. Spach MS, Miller Wt, Dolber PC, Kootsey JM, Sommer JR, Mosher CE. The functional role of structural complexities in the propagation of depolarization in the atrium of the dog. Cardiac conduction disturbances due to discontinuities of effective axial resistivity. Circ Res. 1982;50:175–191. [PubMed: 7055853]
3. Kadish A, Shinnar M, Moore EN, Levine JH, Balke CW, Spear JF. Interaction of fiber orientation and direction of impulse propagation with anatomic barriers in anisotropic canine myocardium. Circulation. 1988;78:1478–1494. [PubMed: 3191601]
4. Spach MS. Anisotropic structural complexities in the genesis of reentrant arrhythmias. Circulation. 1991;84:1447–1450. [PubMed: 1884469]

5. Hocini M, Ho SY, Kawara T, Linnenbank AC, Potse M, Shah D, Jais P, Janse MJ, Haissaguerre M, de Bakker JMT. Electrical conduction in canine pulmonary veins: electrophysiological and anatomic correlation. Circulation. 2002;105:2442–2448. [PubMed: 12021234]
6. Maesen B, Zeemering S, Afonso C, Eckstein J, Burton R a B, van Hunnik A, Stuckey DJ, Tyler D, Maessen J, Grau V, Verheule S, Kohl P, Schotten U. Rearrangement of atrial bundle architecture and consequent changes in anisotropy of conduction constitute the 3-dimensional substrate for atrial fibrillation. Circ Arrhythm Electrophysiol. 2013;6:967–975. [PubMed: 23969531]
7. Klos M, Calvo D, Yamazaki M, Zlochiver S, Mironov S, Cabrera J, Sanchez-quintana D, Jalife J, Berenfeld O, Kalifa J. Atrial Septopulmonary Bundle of the Posterior Left Atrium Provides a Substrate for Atrial Fibrillation Initiation in a Model of Vagally Mediated Pulmonary Vein Tachycardia of the Structurally Normal Heart. Circ Arrhythm Electrophysiol. 2008;1:175–183. [PubMed: 19609369]
8. Berenfeld O Frequency-Dependent Breakdown of Wave Propagation Into Fibrillatory Conduction Across the Pectinate Muscle Network in the Isolated Sheep Right Atrium. Circ Res. 2002;90:1173–1180. [PubMed: 12065320]
9. Ho SY, Sanchez-quintana D, Cabrera JA, Anderson RH. Anatomy of the Left Atrium : Implications for Radiofrequency Ablation of Atrial Fibrillation. J Cardiovasc Electrophysiol. 1999;10:1525–1534. [PubMed: 10571372]
10. Nathan H, Eliakim M. The junction between the left atrium and the pulmonary veins. An anatomic study of human hearts. Circulation. 1966;34:412–422. [PubMed: 5922708]
11. Ho SY, Anderson RH, Sánchez-Quintana D. Atrial structure and fibres: morphologic bases of atrial conduction. Cardiovasc Res. 2002;54:325–336. [PubMed: 12062338]
12. Ho SY, Cabrera JA, Sanchez-Quintana D. Left atrial anatomy revisited. Circ Arrhythm Electrophysiol. 2012;5:220–228. [PubMed: 22334429]
13. Wang K, Ho SY, Gibson DG, Anderson RH. Architecture of atrial musculature in humans. Br Heart J. 1995;73:559–565. [PubMed: 7626357]
14. Zhao J, Butters TD, Zhang H, Pullan AJ, LeGrice IJ, Sands GB, Smaill BH. An image-based model of atrial muscular architecture: effects of structural anisotropy on electrical activation. Circ Arrhythm Electrophysiol. 2012;5:361–370. [PubMed: 22423141]
15. Kato R, Lickfett L, Meininger G, Dickfeld T, Wu R, Juang G, Angkeow P, LaCorte J, Bluemke D, Berger R, Halperin HR, Calkins H. Pulmonary vein anatomy in patients undergoing catheter ablation of atrial fibrillation: lessons learned by use of magnetic resonance imaging. Circulation. 2003;107:2004–2010. [PubMed: 12681994]
16. Marom EM, Herndon JE, Kim YH, McAdams HP. Variations in pulmonary venous drainage to the left atrium: implications for radiofrequency ablation. Radiology. 2004;230:824–829. [PubMed: 14739316]
17. Stejskal EO, Tanner JE. Spin diffusion measurements: spin echoes in the presence of a time-dependent field gradient. Chem Phys. 1965;42:288–292.
18. Basser PJ, Mattiello J, Lebihan D. MR diffusion tensor spectroscopy and imaging. Biophys J. 1994;66:259. [PubMed: 8130344]
19. Mori S, Zhang J. Principles of Diffusion Tensor Imaging and Its Applications to Basic Neuroscience Research. Neuron. 2006;51:527–539. [PubMed: 16950152]
20. Koh DM, Collins DJ. Diffusion-weighted MRI in the body: Applications and challenges in oncology. Am J Roentgenol. 2007;188:1622–1635. [PubMed: 17515386]
21. Sosnovik DE, Wang R, Dai G, Reese TG, Wedeen VJ. Diffusion MR tractography of the heart. J Cardiovasc Magn Reson. 2009;11:47. [PubMed: 19912654]
22. Helm PA, Younes L, Beg MF, Ennis DB, Leclercq C, Faris OP, McVeigh E, Kass D, Miller MI, Winslow RL. Evidence of structural remodeling in the dyssynchronous failing heart. Circ Res. 2006;98:125–132. [PubMed: 16339482]
23. Chen J, Song S-K, Liu W, McLean M, Allen JS, Tan J, Wickline S a, Yu X Remodeling of cardiac fiber structure after infarction in rats quantified with diffusion tensor MRI. Am J Physiol Heart Circ Physiol. 2003;285:H946–H954. [PubMed: 12763752]

24. Helm PA, Tseng H-J, Younes L, McVeigh ER, Winslow RL. Ex vivo 3D diffusion tensor imaging and quantification of cardiac laminar structure. Magn Reson Med. 2005;54:850–859. [PubMed: 16149057]
25. Lombaert H, Peyrat J-MM, Croisille P, Rapacchi S, Fanton L, Cheriet F, Clarysse P, Magnin I, Delingette H, Ayache N. Human atlas of the cardiac fiber architecture: study on a healthy population. IEEE Trans Med Imaging. 2012;31:1436–1447. [PubMed: 22481815]
26. Scollan DF, Holmes A, Winslow R, Forder J. Histological validation of myocardial microstructure obtained from diffusion tensor magnetic resonance imaging. Am J Physiol Circ Physiol. 1998;275:H2308–H2318.
27. Hsu EW, Muzikant AL, Matulevicius SA, Penland RC, Henriquez CS. Magnetic resonance myocardial fiber-orientation mapping with direct histological correlation. Am J Physiol Circ Physiol. 1998;274:H1627–H1634.
28. Kung GL, Nguyen TC, Itoh A, Skare S, Ingels NB, Miller DC, Ennis DB. The presence of two local myocardial sheet populations confirmed by diffusion tensor MRI and histological validation. J Magn Reson Imaging. 2011;34:1080–1091. [PubMed: 21932362]
29. Bernus O, Radjenovic A, Trew ML, LeGrice IJ, Sands GB, Magee DR, Smaill BH, Gilbert SH. Comparison of diffusion tensor imaging by cardiovascular magnetic resonance and gadolinium enhanced 3D image intensity approaches to investigation of structural anisotropy in explanted rat hearts. J Cardiovasc Magn Reson. 2015;17:1–27. [PubMed: 25589308]
30. Jiang H, van Zijl PC, Kim J, Pearlson GD, Mori S. DtiStudio: resource program for diffusion tensor computation and fiber bundle tracking. Comput Methods Programs Biomed. 2006;81:106–116. [PubMed: 16413083]
31. Wang R, Benner T, Sorensen AG, Wedeen VJ. Diffusion Toolkit : A Software Package for Diffusion Imaging Data Processing and Tractography. Proc Intl Soc Mag Reson Med. 2007;15:3720.
32. Papez JW. Heart musculature of the atria. Am J Anat. 1920;27:255–285.
33. Bachmann G The inter-auricular time interval. Am J Physiol. 1916;41:1016.
34. Nielsen PM, Le Grice IJ, Smaill BH, Hunter PJ. Mathematical model of geometry and fibrous structure of the heart. Am J Physiol. 1991;260:H1365–H1378. [PubMed: 2012234]
35. Hamabe A, Okuyama Y, Miyauchi Y, Zhou S, Pak HN, Karagueuzian HS, Fishbein MC, Chen PS. Correlation between anatomy and electrical activation in canine pulmonary veins. Circulation. 2003;107:1550–1555. [PubMed: 12654615]
36. Markides V Characterization of Left Atrial Activation in the Intact Human Heart. Circulation. 2003;107:733–739. [PubMed: 12578877]
37. Haissaguerre M, Hocini M, Denis A, Shah AJ, Komatsu Y, Yamashita S, Daly M, Amraoui S, Zellerhoff S, Picat MQ, Quotb A, Jesel L, Lim H, Ploux S, Bordachar P, Attuel G, Meillet V, Ritter P, Derval N, Sacher F, Bernus O, Cochet H, Jais P, Dubois R. Driver domains in persistent atrial fibrillation. Circulation. 2014;130:530–538. [PubMed: 25028391]
38. Narayan SM, Krummen DE, Shivkumar K, Clopton P, Rappel WJ, Miller JM. Treatment of atrial fibrillation by the ablation of localized sources: CONFIRM (Conventional Ablation for Atrial Fibrillation with or Without Focal Impulse and Rotor Modulation) trial. J Am Coll Cardiol. 2012;60:628–636. [PubMed: 22818076]
39. Lamata P, Casero R, Carapella V, Niederer S a, Bishop MJ, Schneider JE, Kohl P, Grau V. Images as drivers of progress in cardiac computational modelling. Prog Biophys Mol Biol. 2014;115:198–212. [PubMed: 25117497]
40. Trayanova NA. Whole-heart modeling: applications to cardiac electrophysiology and electromechanics. Circ Res. 2011;108:113–128. [PubMed: 21212393]
41. Labarthe S, Bayer J, Coudière Y, Henry J, Cochet H, Jaïs P, Vigmond E. A bilayer model of human atria: mathematical background, construction, and assessment. Europace. 2014;16 Suppl 4:iv21–iv29. [PubMed: 25362166]
42. Seemann G, Höper C, Sachse FB, Dössel O, Holden AV, Zhang H. Heterogeneous three-dimensional anatomical and electrophysiological model of human atria. Philos Trans A Math Phys Eng Sci. 2006;364:1465–1481. [PubMed: 16766355]

43. McDowell KS, Vadakkumpadan F, Blake R, Blauer J, Plank G, MacLeod RS, Trayanova N a. Methodology for patient-specific modeling of atrial fibrosis as a substrate for atrial fibrillation. J Electrocardiol. 2012;45:640–645. [PubMed: 22999492]
44. Krüger MW. Personalized Multi-Scale Modeling of the Atria. Vol 19 KIT Scientific Publishing; 2013.
45. Gonzales MJ, Vincent KP, Rappel W-J, Narayan SM, McCulloch AD. Structural contributions to fibrillatory rotors in a patient-derived computational model of the atria. Europace. 2014;16 Suppl 4:iv3–iv10. [PubMed: 25362167]
46. Beg MF, Helm PA, McVeigh E, Miller MI, Winslow RL. Computational cardiac anatomy using MRI. Magn Reson Med. 2004;52:1167–1174. [PubMed: 15508155]
47. Nielles-Vallespin S, Mekkaoui C, Gatehouse P, Reese TG, Keegan J, Ferreira PF, Collins S, Speier P, Feiweier T, Silva R. In vivo diffusion tensor MRI of the human heart: Reproducibility of breath-hold and navigator-based approaches. Magn Reson Med. 2013;70:454–465. [PubMed: 23001828]
48. Nguyen C, Fan Z, Sharif B, He Y, Dharmakumar R, Berman DS, Li D. In vivo three-dimensional high resolution cardiac diffusion-weighted MRI: A motion compensated diffusion-prepared balanced steady-state free precession approach. Magn Reson Med. 2013;1267:1257–1267.
49. Gamper U, Boesiger P, Kozerke S. Diffusion imaging of the in vivo heart using spin echoes--considerations on bulk motion sensitivity. Magn Reson Med. 2007;57:331–337. [PubMed: 17260376]

WHAT IS KNOWN

- Accurate knowledge of myofiber architecture in the human atria is paramount to understanding the role of organ structure in atrial electrical activity in health and disease.
- Atrial fiber structure is complex and atrial anatomy varies greatly humans. However, there is a paucity of data regarding three-dimensional fiber orientation in the human atria and its inter-subject variability.

WHAT THE STUDY ADDS

- The application of sub-millimeter DTMRI provides detailed reconstructions of fiber organization in intact human atria and allows for characterization of major fiber bundles as well as transmural fiber orientation.
- Despite variation in the exact location of the fiber bundles, a set of major fiber bundles were found to be consistent across most of the subjects.
- Transmural fiber patterns showed variation throughout the atria, demonstrating regional heterogeneity in the extent of fiber angle differences across the wall.

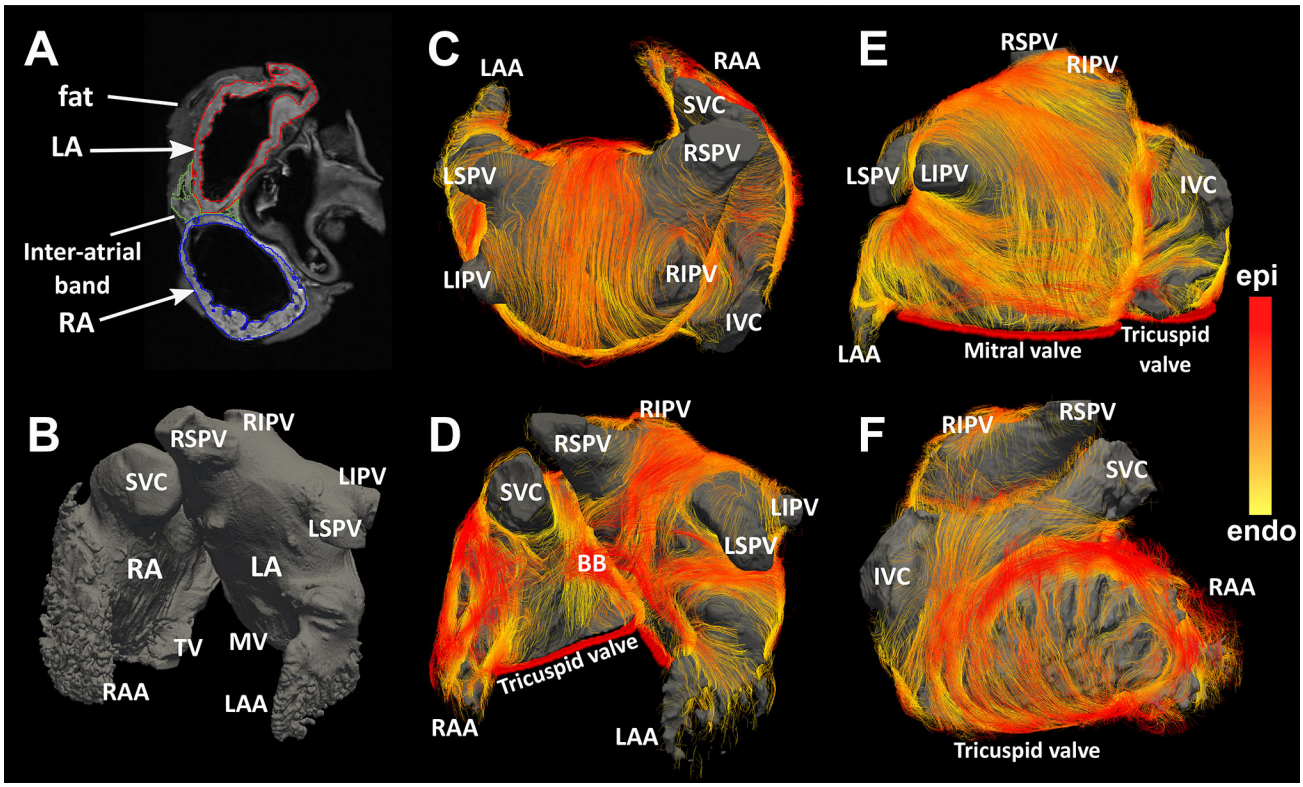

Figure 1:

Acquired geometry and fiber visualization results in human atria specimens. (Left panel) Atrial geometry: (**A**) Short-axis view of a non-diffusion weighted image (b0) with superimposed segmentation of left atrium (LA, red), right atrium (RA, blue) and inter-atrial bundles (green). Fat tissue surrounding the atria is excluded from the segmentation. (**B**) Anterior view of left and right atria created from T1-weighted images; the dark grey volume represents lumen. (Right panel): Fiber visualization using tractography. (**C**) Posterior view of atrial roof. (**D**) Anterior view. (**E**) Inferior and left lateral view. (**F**) View of right atrium. Color encodes the local distance to the endocardial shell: yellow is the endocardial layer, and red is the epicardial layer. (LIPV: Left inferior pulmonary vein, LSPV: Left superior pulmonary vein, RIPV: Right inferior pulmonary vein, RSPV: Right superior pulmonary vein, LAA: Left atrial appendage, RAA: Right atrial appendage, IVC: inferior vena cava, SVC: superior vena cava, MV: Mitral valve, TV: Tricuspid valve, BB: Bachman bundle)

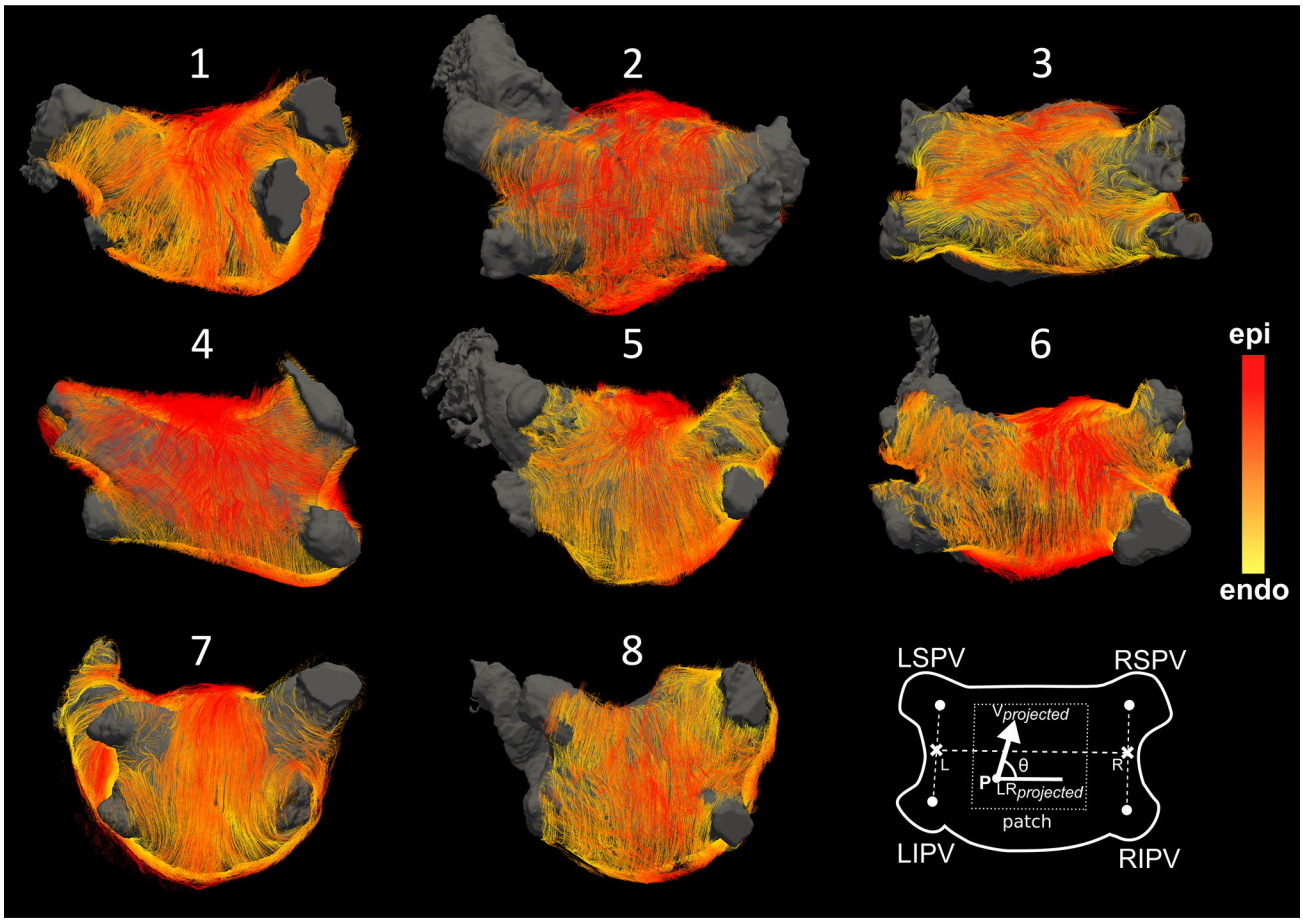

Figure 2:

Fiber tractography in eight hearts as viewed posteriorly over the roof of the LA. The lumen of each atrium is colored gray. Color-coding is as in Figure 1C–F. The schematic at the bottom right shows the “horizontal” direction defined by the four origins of the PVs, as described in Methods. Fiber angles on the roof of the posterior wall are measured with respect to that horizontal (marked LR in schematic). Average fiber angles at the roof were calculated in the region outlined by the dashed box.

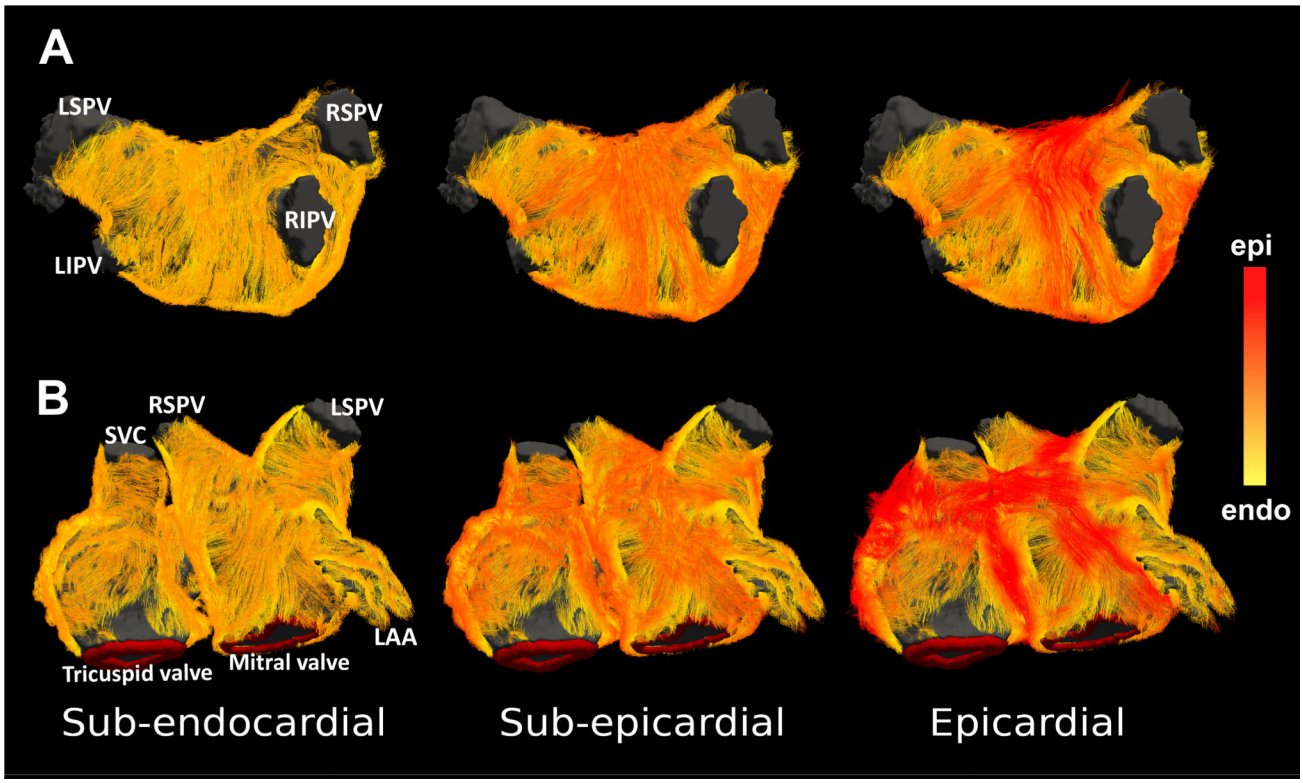

Figure 3:

Fiber tractography of human atria (specimen 1) at different transmural layers as viewed from the Posterior (**A**) and Anterior (**B**) sides. The right column presents the original tracts. Left and middle columns represent the same results with sub-endocardial and sub-epicardial cuts, such that the outer layer fibers (at higher distances from the endocardium) have been removed from the visualization. The tracts have been visualized at a higher density (less culling down – see Supplementary Methods) in comparison to Figs 1 and 2. The color-encoding is based on the distance from the endocardial shell.

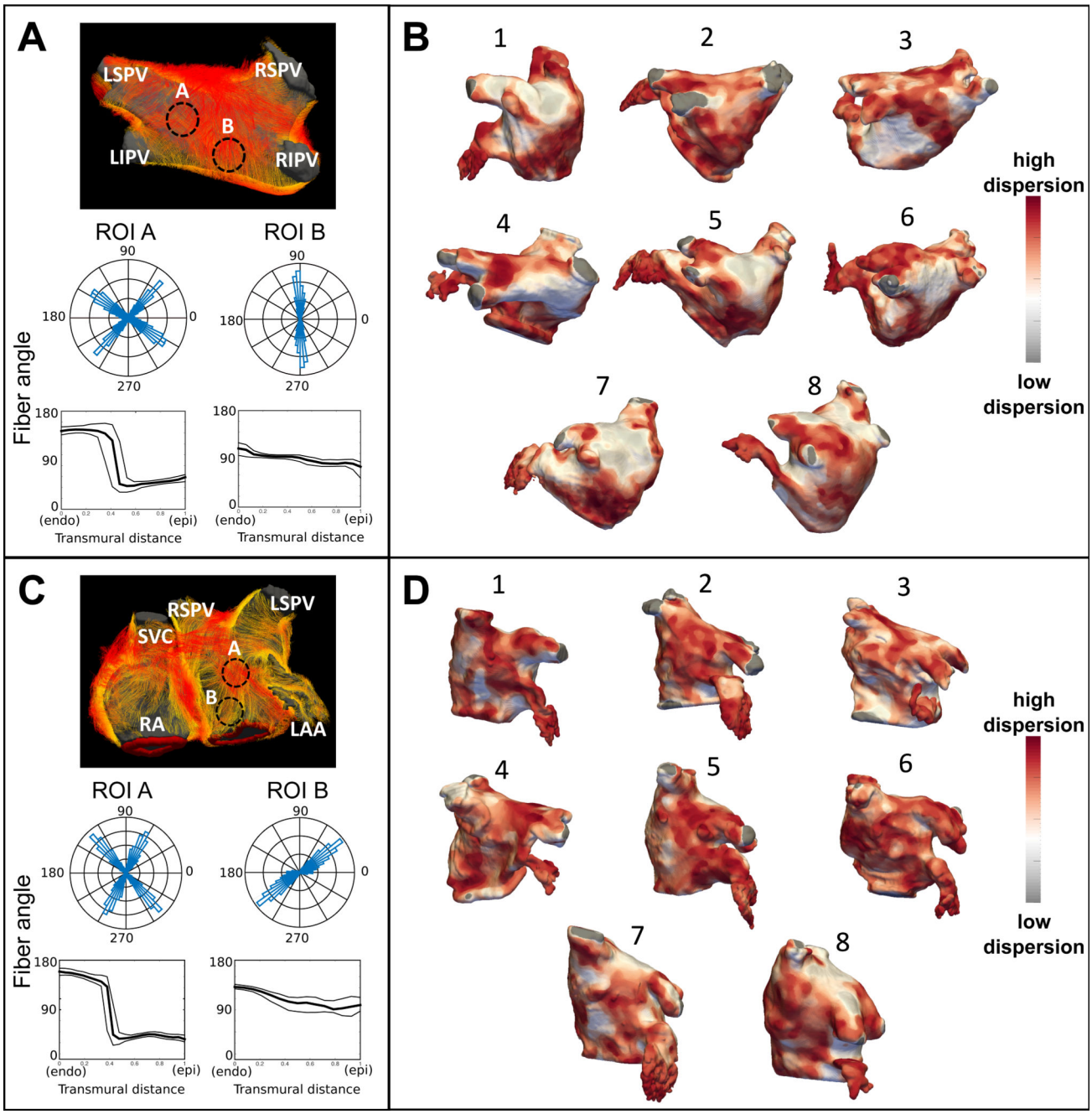

Figure 4:

Regional changes in fiber orientation across the atrial wall. (**A**) (top) posterior view of the LA of specimen 4; (middle), a histogram of the transmural distribution of fiber angles from two ROIs; and (bottom), the transmural profile of fiber angles as a function of atrial wall depth in ROIs A and B. (**B**) Posterior lateral view of the maps of transmural angle dispersion for the eight specimens. (**C**) Same as (**A**) in sample 1. (**D**) Anterior view of the maps of transmural angle dispersion.

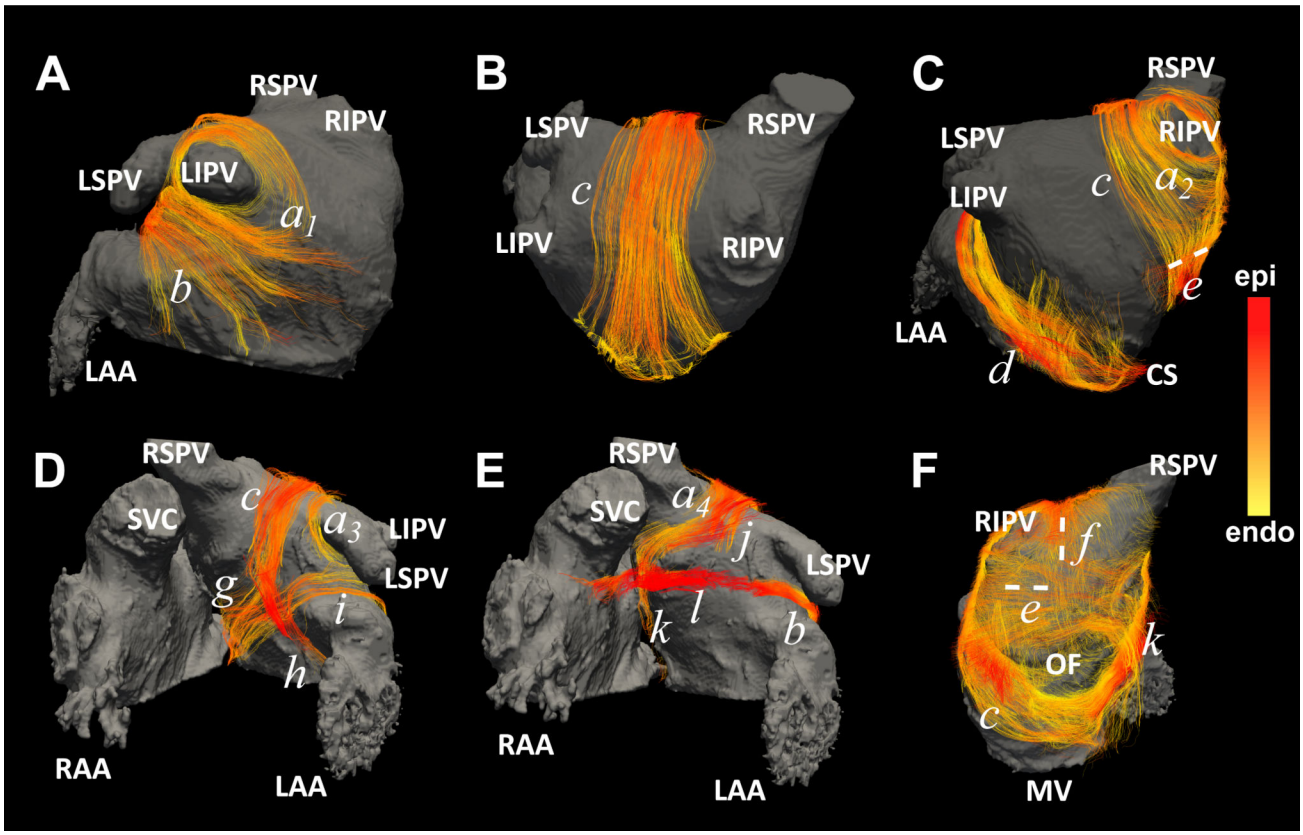

Figure 5:

The major fiber bundles in the human LA. (**A**-**C**) Posterior; (**D**,**E**) Anterior view, and (**F**) Septum. The individual bundles are denoted a-l in heart 7.

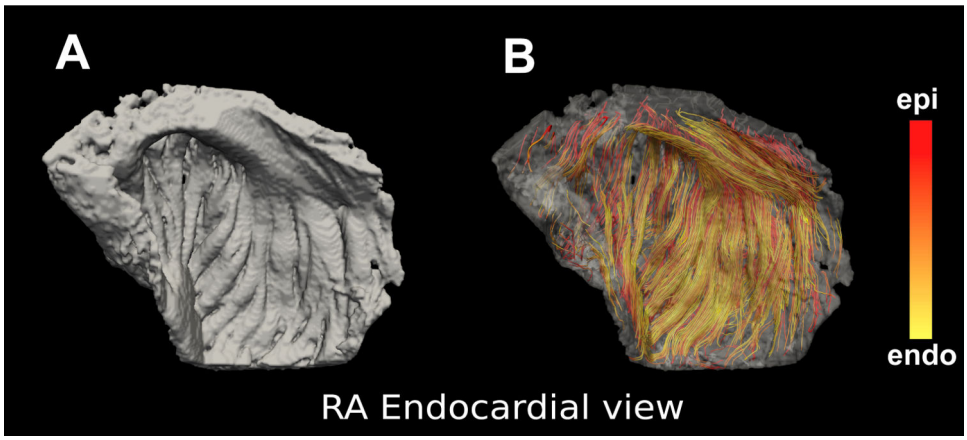

Figure 6:

Endocardial view of the right atrium of specimen 4. (**A**) 3D rendering of trabeculated structure reconstructed from non-diffusion weighted MR images and (**B**) the corresponding fiber tracts overlaid on top. The pectinate muscles and crista terminalis of the right atrium are manifested as dense tracts in tractography results. The orientation of these fiber tracts follows the trabeculated structure of the endocardial wall (**A**).

Table 1:

Subject characteristics and measured fiber angles on the roof of the left atria for the post-mortem heart samples used in this study. The statistics were calculated based on the fiber angles measured within the patch shown in Figure 2. The “angle spread” is the root mean square deviation of the fiber angles.

Heart Name	Age/Sex	Cardiac disease status	Angle mean (°)	Angle spread (°)
Heart 1	93/F	MI	97	27
Heart 2	67/F	MI	98	26
Heart 3	90/F	Normal	168	36
Heart 4	76/M	MI	105	28
Heart 5	76/F	Normal	95	27
Heart 6	94/F	AF	100	19
Heart 7	86/M	AF	99	12
Heart 8	55/M	Normal	101	18

AF: Atrial Fibrillation, MI: Myocardial Infarction, M: Male, F: Female